PCCP

Accepted Manuscript

This article can be cited before page numbers have been issued, to do this please use: Z. Liu, V. S. Nguyen, J. Harvey, J. Muller and J. Peeters, *Phys. Chem. Chem. Phys.*, 2018, DOI: 10.1039/C7CP08421H.

ROYAL SOCIETY OF CHEMISTRY

rsc.li/pccp

View Article Online
DOI: 10.1039/C7CP08421H

PCCP

ARTICLE

The photolysis of α-hydroperoxycarbonyls

Zhen Liu[b], Vinh Son Nguyen[a], Jeremy Harvey[a], Jean-François Müller[c], and Jozef Peeters*[a]

Received 00th November 2017,
Accepted 00th November 2017

DOI: 10.1039/x0xx00000x

www.rsc.org/

In this work, we theoretically elucidated the mechanism and predicted the major products of the photolysis of α-hydroperoxycarbonyls, known to be products of the atmospheric oxidation of biogenic volatile organic compounds (BVOC) and components of secondary organic aerosol (SOA) in rural and remote areas. Using 2-hydroperoxypropanal $OCHCH(OOH)CH_3$ as a model compound, we show that the likely major photolysis mechanism is a fast 1,5 H-shift in the initially excited singlet S_1 state followed by spontaneous elimination of singlet oxygen to yield an enol $HOCH=CHCH_3$, while intersystem crossing (ISC) to the triplet T_1 state and C–C scission into $HC^{\bullet}O + HOOC^{\bullet}HCH_3$ followed by expulsion of a hydroxyl radical from the unstable $HOOC^{\bullet}HCH_3$ is another product channel. The direct S_1 reaction was found to occur at such a high rate that the quantum yield in atmospheric conditions is expected to approach unity. In the atmosphere, the enol should generally react with OH radicals or tautomerize into the more stable carbonyl $O=CH-CH_2CH_3$. Vinylalcohol is shown to be a major end product of the photolysis of hydroperoxyacetaldehyde, an isoprene oxidation product. Taking into account also the important enhancement of the absorption cross sections over those of the constituent monofunctional compounds as observed for the analogous β-ketohydroperoxides, (*J. Photochem. Photobiol. A Chem.*, 2000, 134, 119-125; ref. 1) the atmospheric photolysis rate of α-hydroperoxycarbonyls was estimated to be in the range of (1 to 5) × 10^{-4} s^{-1}, generally faster than the rate of their OH reactions.

Introduction

The oxidation of organic compounds released in large amounts by the biosphere and by anthropogenic activities generates a plethora of products with multiple oxygenated functional groups, among which the hydroperoxide, nitrate, carbonyl and alcohol groups are especially prominent.[2] Those polyfunctional compounds are essential to the formation of Secondary Organic Aerosol (SOA), a large component of particulate matter in the atmosphere. Multifunctional hydroperoxides, in particular, were singled out as a major SOA components in rural conditions[3-6] owing to their low volatility,[7] their high solubility in water[8] and their large rate of production through reactions of organic peroxy radicals with the hydroperoxy radical. More recently, autoxidation via H-shifts in organic peroxy radicals was proposed to play a substantial role as a source of multifunctional hydroperoxides and carbonyls[9-11] and to be a uniquely efficient pathway for formation of extremely low-volatility compounds (ELVOCs) bearing multiple hydroperoxide groups, believed to play an essential role in particle formation and growth over boreal forests.[12] Carbonyl hydroperoxides can be expected to constitute a significant fraction of those ELVOCs and of the higher-volatility intermediates involved in their formation.

Isoprene oxidation is not a large source of ELVOCs,[13] but it has been shown in laboratory studies (mostly at Caltech) to form carbonyl hydroperoxides through several pathways, including the OH-induced oxidation of methylvinylketone (MVK)[14] and of isoprene hydroxyhydroperoxides,[15-16] the nitrate-initiated oxidation of isoprene,[17] and the chemistry following the 1,6 H-shift in *Z*-δ-hydroxyperoxy isoprenyl (*Z*-δ-ISOPO2) radicals[18] as originally proposed in the Leuven Isoprene Mechanism LIM1.[19] Table S3 (Electronic Supplementary Information, ESI) lists the major hydroperoxy-carbonyls identified so far in the oxidation of isoprene (excluding the *conjugated*

[a] *Department of Chemistry, University of Leuven, Celestijnenlaan 200F, B-3001 Leuven, Belgium.*
[b] *State Key Laboratory of Chemical Engineering, East China University of Science and Technology, Meilong Road 130, 200237, Shanghai, China.*
[c] *Royal Belgian Institute for Space Aeronomy, Avenue Circulaire 3, B-1180 Brussels, Belgium.*
*Email: Jozef.Peeters@kuleuven.be
Electronic Supplementary Information (ESI) available. Geometries and Cartesian coordinates; Complete Active Space computations; cross section and actinic flux data, See DOI: 10.1039/x0xx00000x

View Article Online
DOI: 10.1039/C7CP08421H
ARTICLE PCCP

hydroperoxyaldehydes HPALDs[9-10]) as well as those formed in the OH-oxidation of simple carbonyls.

Although the total photolysis rate of multifunctional carbonyls is generally calculated in models[20-21] as the sum of the rates for structurally similar monofunctional compounds, recent work has shown that interactions between chromophores can result in strong enhancements in the quantum yields (e.g. for the HPALDs[22-23] and for carbonyl nitrates[24-25]) and in the absorption cross sections (e.g. for the carbonyl nitrates[25-26]). Recently, the α-ketohydroperoxide formed from MVK+OH was found to photodissociate rapidly in the laboratory[14] and its photolysis lifetime was estimated to be short under atmospheric conditions (<< 1 day). This high photodissociation rate indicates high quantum yields, as we proposed for α-hydroperoxycarbonyls,[19] and/or enhanced absorption cross sections, as found in the laboratory for hexyl-ketohydroperoxides in solution in acetonitrile.[1] The products of hydroperoxycarbonyl photolysis are not known; it was assumed by Praske[14] that the α-ketohydroperoxide formed from MVK+OH photolyzes by breaking of the O—O bond in the hydroperoxide moiety to yield the hydroxyl radical and an oxy radical.

In this work, we aim (1) to fully elucidate at high levels of theory the detailed mechanism and predict the main products of the photolysis of 2-hydroperoxy-propanal (2-HPP) as a model compound for α-hydroperoxycarbonyls, (2) propose a methodology for estimating the photolysis rates of hydroperoxycarbonyls, based on existing laboratory data, and (3) briefly examine the possible atmospheric implications of our results.

Methodologies

A conformational search of ground state 2-HPP S_0 was first performed using a molecular mechanics (MM) conformational analysis with the Tinker program.[27] A suitable MM atom type was assigned to each atom based on the MMFF force field definition. Initial structures obtained at the MM level were then optimized using density functional theory (DFT), with the M06-2X-D3 functional, the 6-311++G(2d,p) basis set, and the Gaussian 09[28] program. The electronically-excited S_1 state of 2-HPP S_1, and the corresponding transition state for 1,5 H-shift, were studied at the TD-M06-2X-D3/6-311++G(2d,p) level of theory. The relative energies are given with respect to the global minimum of the ground state 2-HPP S_0. An ultrafine DFT integration grid was employed in order to minimize numerical error for the vibrational frequencies. Where appropriate, single-point CCSD(T)-F12/cc-pVDZ-F12 energies were computed with the ORCA 4.0 program.[29] A restricted HF-reference wavefunction was used for the coupled cluster calculations on closed-shell molecules (RHF/CCSD(T)), while an open-shell HF-reference wavefunction was adopted for the unrestricted coupled cluster calculations on open-shell molecules (UHF/UCCSD(T)). The important 1,5 H-shift in the S_1† was also studied for the simpler homologue hydroperoxyacetaldehyde (OCH-CH_2OOH, HPAC) using the multi-reference CASSCF method with a large active space of 16 electrons in 12 orbitals. This active space contains all the important bonding and anti-bonding orbitals of the carbonyl and hydroperoxy groups, and test calculations also showed that it can also provide a balanced description of the hydrogen transfer TS and of subsequent steps. A graphical representation of these orbitals is included in the Electronic Supplementary information (Figure S8, ESI). The geometry optimizations for the HPAC model reaction were performed at the CASSCF(16,12)/DZP level using a state-averaged procedure in which the two lowest-energy singlet states were equally weighted, with gradients computed for the excited state. The energies were then refined by single-point multistate (MS) CASPT2/def2-TZVPP calculations using the state-averaged CASSCF wave functions as reference. It should be noted that for HPAC, the favourable comparison of the TD-M06-2X-D3/6-311++G(2d,p) energy of the S_1 state and of the energy barrier for the 1,5 H-shift (Figure S5, ESI) to the energies at the higher CASPT2(16,12)//CASSCF(16,12) level (Figure S9, ESI), supports the reliability of TD-M06-2X-D3 for S_1-excited hydroperoxyaldehydes and in particular for the crucial energy barrier of the 1,5 H-shift. All multi-reference computations including the geometry optimizations were performed with the Molpro 2012.1 program package.[30]

The statistical-kinetics rates for the chemically activated reactions of interest were derived using RRKM theory.[31-32] The micro-canonical rate coefficients were obtained using:

$$k\left(E_v\right) = \alpha \times G^{\neq}\left(E_v - E^{\neq}\right) / \left(h \times N\left(E_v\right)\right)$$

in which α is the reaction path degeneracy, h Planck's constant, $E^{\neq}$ the TS energy, E_v the vibrational energy of the reacting activated intermediate, $N(E_v)$ its density of

View Article Online
DOI: 10.1039/C7CP08421H
PCCP ARTICLE

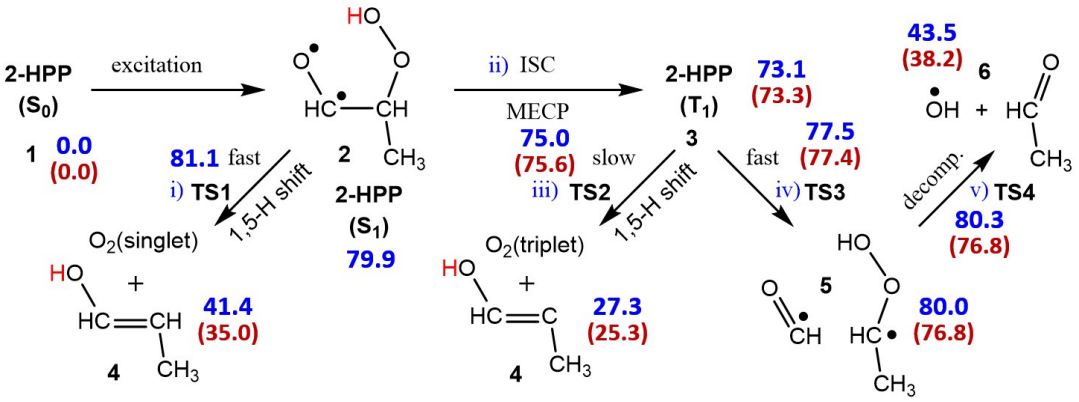

Figure 1. The plausible reactions of the excited 2-HPP. The relative energies (with *ZPVE*) in blue are computed at M06-2X-D3/6-311++G(2d,p) level of theory for ground state singlet, doublet, and triplet species, and at TD-M06-2X-D3/6-311++G(2d,p) level for the exited S_1 species. The numbers in red inside the parentheses are the CCSD(T)-F12 energies with inclusion of TD-M06-2X-D3 *ZPVE*. All the energies (kcal mol^{-1}) are relative to the global minimum 2-HPP(1a).

vibrational states, and $G^{\neq}(E_v\text{-}E^{\neq})$ the sum of accessible vibrational states of the TS. Both the latter terms were evaluated by exact count,[32] based on the unscaled M06-2X vibrational frequencies. It was ascertained for some of the unimolecular reactions that frequency-scaling by a factor of 0.97 only has a very minor effect on rate constants, smaller than the error margin due to the uncertainties on the energies. For all principal reactions, the rates were estimated at the average vibrational energy.

Results and Discussion

Photolysis of 2-hydroperoxy-propanal. The atmospheric photolysis of 2-HPP is expected to occur as for other aldehydes by excitation of the S_0 ground state to the first excited singlet state S_1, by absorption of solar radiation in the range 300-340 nm. Since the rate of the subsequent photo-physical and/or chemical processes depends on the internal energy content of the $S_1^{\dagger}$ molecule, at least an estimate of the average nascent vibration energy is needed. To that end, the energy of S_1 relative to S_0 is required as well as the product of the absorption cross section $\sigma(\lambda)$ and the solar actinic flux $F(\lambda)$ at the earth's surface (taken for a 30° solar zenith angle) as functions of wavelength λ. As detailed below, the computed TD-M06-2X-D3/6-311++G(2d,p) energy including *ZPVE* of the lowest conformer of S_1 is 79.9 kcal mol^{-1} relative to the lowest S_0 conformer. The absorption cross section $\sigma(\lambda)$ of 2-hydroperoxy-propanal is not known; as discussed in the section on photolysis rates, it was estimated assuming additivity of the cross sections of the monofunctional compounds propanal and the alkylhydroperoxide CH_3OOH, but taking into account a λ-dependent enhancement factor derived from measured $\sigma(\lambda)$ data on similar hydroperoxycarbonyls.[1] Referring to Figure 5 in the photolysis rate section, the enhancement shifts the maximum of the product $\sigma(\lambda) \times F(\lambda)$ slightly, from 320 to 325 nm, but increases the product value by about an order of magnitude. Adding in the thermal vibration energy of S_0 of nearly 3 kcal mol^{-1} at 298K, the average nascent vibration energy of the $S_1^{\dagger}$ state is predicted to be ≈12 kcal mol^{-1}, with 90% of excited molecules having E_{vib} in the range 12±5 kcal mol^{-1}.

As detailed below and depicted (partly) in Figure 1, the possible subsequent processes/reactions of $S_1^{\dagger}$ (**2**) are: direct photolysis through the $S_1^{\dagger}$ state by a 1,5 H-shift followed by singlet O_2 elimination to yield an enol; intersystem crossing (ISC) $S_1 \rightarrow T_1$ and fast dissociation of the activated $T_1^{\dagger}$ into $HC^{\bullet}O$ + $HOOC^{\bullet}H\text{-}CH_3$; internal conversion (IC) $S_1 \rightarrow S_0$ followed possibly by impulsive dissociation of the highly vibrationally activated $S_0^{\dagger}$; collisional deactivation of $S_1^{\dagger}$ to S_1 at an expected rate of order 10^9 s^{-1} at 1 atm.; or collisional quenching to ground state $S_0^{(\dagger)}$.

A1. Direct photolysis mechanism through the S_1 state. A first photolysis mechanism occurs directly through the vibrationally activated $S_1^{\dagger}$ state by 1,5 H-shift of the

View Article Online
DOI: 10.1039/C7CP08421H
ARTICLE PCCP

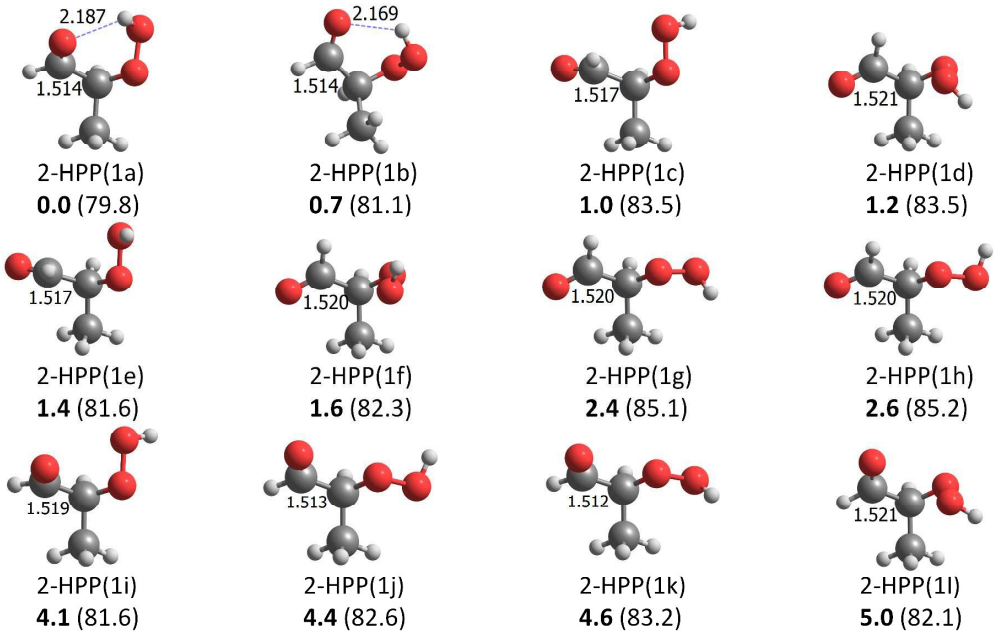

Figure 2. Geometries and relative energies *E* of the conformers of 2-HPP(**1**) in ground S_0 state, at the M06-2X-D3/6-311++G(2d,p) level of theory. The relative energies inside the parentheses are for the S_1 structures by direct excitation of the S_0 conformers, calculated at TD-M06-2X-D3/6-311++G(2d,p) level of theory. All the energies (kcal mol^{-1}, with *ZPVE*) are relative to the global minimum 2-HPP(1a).

hydroperoxide H atom. This shift is followed by spontaneous elimination of singlet O_2 to yield an enol, **4**, as detailed in the ESI, such that the overall reaction can be represented as a Norrish type II mechanism:

$$O^{\bullet}C^{\bullet}H\text{-}CH(OOH)\text{-}CH_3\,(S_1) \rightarrow {}^1O_2 + HOCH{=}CH\text{-}CH_3 \quad \text{(R. i)}$$

Obviously, the barrier to the H-shift depends on the conformation of the reacting S_1 molecule. Therefore, a detailed conformational analysis was carried out, not only of S_1, but firstly of ground state 2-HPP(**1**) S_0 in order to determine the thermal population fractions — which will also be the formation fractions of the directly generated S_1 conformers, in the assumption of equal absorption cross sections for all S_0 conformers.

Figure 2 depicts the 12 identified conformers of S_0; of these, 2 show an H-bond and are also the most stable conformers: 2-HPP(1a) S_0 and 2-HPP(1b) S_0. The computed relative energies with inclusion of *ZPVE* are shown for the S_0 and resulting S_1 structures, optimized at the M06-2X-D3/6-311++g(2d,p) and TD-M06-2X-D3/6-311++g(2d,p) levels, respectively; the energies are all relative to the lowest-lying

Table 1. Relative Gibbs free energies (kcal mol^{-1}) and thermal population fractions (%) for all the 12 conformers of ground state 2-HPP(**1**).

	Δ*G* (298 K)[a]	*thermal population fractions* (%)
2-HPP(1a)	0.0	24.3
2-HPP(1b)	0.9	5.4
2-HPP(1c)	-0.1	26.8
2-HPP(1d)	0.7	7.3
2-HPP(1e)	0.0	26.0
2-HPP(1f)	0.8	6.2
2-HPP(1g)	1.6	1.8
2-HPP(1h)	1.5	2.0
2-HPP(1i)	3.1	0.1
2-HPP(1j)	3.4	0.1
2-HPP(1k)	3.5	0.0
2-HPP(1l)	4.4	0.0

[a]Δ*G*, the relative Gibbs free energy (298 K) at CCSD(T)-F12/cc-pVDZ-F12//M06-2X-D3/6-311++G(2d,p) level of theory. Note that the order is different from that of the M06-2X-D3/6-311++G(2d,p) relative energies in Figure 1.

View Article Online
DOI: 10.1039/C7CP08421H
PCCP ARTICLE

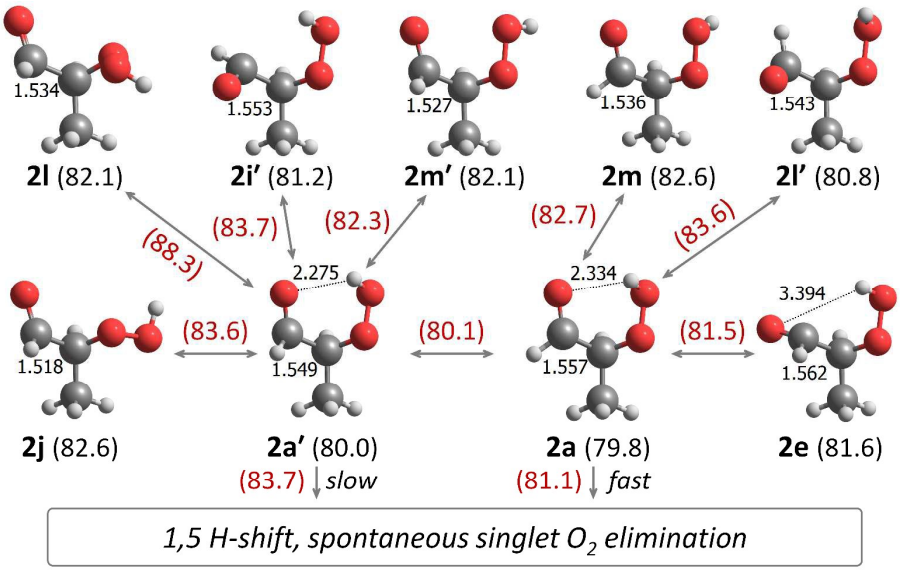

Figure 3. All the interconversion of various 2-HPP(**2**) S_1 conformers to 2a and 2a'. A complete schematic representation of the interconversion of 30 S_1 conformers is available in the Supplementary Information (Figure S3). All the energies (kcal mol^{-1}, with *ZPVE*) are at the TD-M06-2X-D3/6-311++G(2d,p) level of theory and are relative to the global minimum 2-HPP(1a).

S_0 conformer 2-HPP(1a). Table 1 lists the thermal population fractions (in percentage) of all the S_0 conformers at 298 K, based on the relative free energies ΔG computed at the CCSD(T)-F12//M06-2X-D3 level. Interestingly, only 3 of the 12 S_0 conformers are heavily populated: 2-HPP(1a), 2-HPP(1c), and 2-HPP(1e), making up together 77% of the total thermal population. The lowest S_1 conformer is 2-HPP(2a) S_1, its energy E at the TD-M06-23X-D3/6-311++g(2d,p) level being 79.9 kcal mol^{-1} above that of its precursor 2-HPP(1a) S_0. This value is compatible with the CCSD(T)-F12//M06-2X-D3 computed energy of the corresponding triplet T_1 state of 73.3 kcal mol^{-1} (Figure 1): the $S_1 - T_1$ difference of 6.6 kcal mol^{-1} is close to the experimental difference of 7.2 kcal mol^{-1} for acetaldehyde.[33-34] In total 30 conformers of the 2-HPP(**2**) S_1 state have been identified and optimized at the TD-M06-23X-D3 level (Figure S1, ESI). They consist of 15 pairs of twins, denoted e.g. as 2a and 2a' (see also Figure 3) that (mostly) differ only by the formyl-hydrogen lying slightly above or slightly below the OCC plane, and that can quickly interconvert over low barriers. Only the hydrogen-bonded conformers 2a, 2a', 2o and 2o' can directly undergo a 1,5 H-shift, over TD-M06-2X-D3 computed barriers of 1.3, 3.7, 4.3, and 1.7 kcal mol^{-1}, respectively; the transition states are depicted in Figure S2. Of the total of 30 conformers, 12, among which 2a, 2c and 2e, are directly generated by excitation of the 12 S_0 conformers, while 18 arise by conversions of the former, as schematically represented in Figure S3. Each conformer can interconvert to 3 to 6 others. As an example, Figure 3 shows the interconversions of the important subpool of conformers directly linked to 2a and 2a', as well as the 1,5 H-shift exit channels of 2a and 2a'. All 140 photo-activated interconversion rate constants, calculated for an average internal energy of 12 kcal mol^{-1} for 2-HPP(2a)-S_1, are tabulated in Table S1, while the rate constants of the activated 1,5 H-shifts of conformers 2a, 2a', 2o and 2o', ranging from 2.9×10^{10} to 3.4×10^{11} s^{-1} are listed in Table S2. The overall rate constant for 1,5 H-shift of the entire pool of interconverting conformers, k(H,overall), was estimated by solving the system of 30 simultaneous linear equations describing the quasi steady-state concentrations — reached within ≈10 ps — of all 30 S_1 conformers, accounting for the fractional initial formation rates of the 12 directly generated conformers, and assuming that all 30 conformers undergo intersystem crossing (ISC) at identical, estimated rates, for which three values in the range $(3 - 30) \times 10^9$ s^{-1} were adopted (see next subsection). The quasi steady-state equations, which are fully justified in atmospheric photochemistry, are shown under Figure S3, while the relevant (overall) rate constants and finally the

View Article Online
DOI: 10.1039/C7CP08421H

ratio of the overall fractions 1,5 H-shift and intersystem crossing are listed in Table S2. Thus, *k*(H,overall) is found to be ≈5 × 10^{10} s^{-1} , and for *k*(ISC) = 1 × 10^{10} s^{-1}, a ratio *k*(H,overall)/*k*(ISC) = 84/16 is obtained, indicating that the 1,5 H-shift is the major exit pathway of activated 2-HPP(**2**) S_1. However, for an unlikely high *k*(ISC) of 1 × 10^{11} s^{-1} , ISC would be faster than 1,5 H-shift.

It may also be noted that *k*(H,overall) is nearly 50 times higher than the ≈10^9 s^{-1} collisional stabilization rate of the $S_1^{\dagger}$ at 1 atm, such that the quantum yield of photolysis through the direct S_1 mechanism may approach unity.

An IRC analysis at the TD-M06-2X-D3 level, aiming to elucidate the overall mechanism of reaction (R.i) and establish its end products, was not successful, because the 1,5 H-shift leads to a region of the potential energy surface corresponding to a singlet biradical, where the singlet closed-shell reference for the TDDFT calculations ceases to be meaningful. Accordingly, this difficult region of the potential energy surface was thoroughly re-explored for the simpler hydroperoxyacetaldehyde (HPAC) homologue OCH-CH_2OOH using the multi-reference CASSCF method which is able in principle to describe both the S_1 and S_0 states correctly to zeroth-order. To obtain more accurate energies, CASPT2 calculations were also performed. Careful convergence tests for both the size of the active space and of the one-particle basis set were carried out in order to determine the energetics in this region as accurately as possible. Details of this work are provided in the ESI. Here, we simply report that, after the 1,5 H-shift reaction of HPAC-S_1, a spontaneous decomposition into an enol and singlet $O_2(^1\Delta)$ is observed to occur readily without showing a noticeable barrier on the CASPT2 potential energy surface (Figure S9). Therefore, reaction (R.i) can be regarded as a Norrish type II mechanism. Importantly, we also found that the 80.7 kcal mol^{-1} energy of HPAC-S_1 and the 1.8 kcal mol^{-1} energy barrier for the 1,5-H-shift at the TD-M06-2X-D3 level compare favourably with the higher-level CASPT2(16,12)//CASSCF(16/12) energies of 81.7 and 2.2 kcal/mol, respectively, which supports the reliability of the TD-M06-2X-D3 method for S_1-excited hydroperoxyaldehydes and their 1,5 H-shift reactions, investigated in this work.

A2. Photolysis through the 2-HPP T_1 and 2-HPP S_0 states . A second photolysis mechanism, similar to that for acetaldehyde,[35-36] among others, proceeds through intersystem crossing (ISC) of S_1 to the triplet state T_1 , **3**, (Figure 1):

$$O^{\bullet}C^{\bullet}H\text{-}CH(OOH)\text{-}CH_3\,(S_1) \rightarrow O^{\bullet}C^{\bullet}H\text{-}CH(OOH)\text{-}CH_3\,(T_1) \qquad (R.ii)$$

As S_1 suffers almost no collisional energy loss at 1 atm during its short lifetime (see above), the resulting activated $T_1^{\dagger}$ will initially contain some 18 kcal mol^{-1} vibrational energy on average. The triplet biradical can react mainly in two ways: 1,5-H shift and concerted triplet O_2 elimination via a Norrish type II mechanism to yield the enol **4**, similar to the S_1 reaction (R.i) above:

$$O^{\bullet}C^{\bullet}H\text{-}CH(OOH)\text{-}CH_3\,(T_1) \rightarrow {}^3O_2 + HOCH{=}CH\text{-}CH_3 \qquad (R.iii)$$

or T_1 can dissociate by β C-C scission, similar to the principal T_1 state reaction in the photolysis of acetaldehyde,[37-39] propanal[40] and *i*-butanal[41] around 280 – 330 nm.

$$O^{\bullet}C^{\bullet}H\text{-}CH(OOH)\text{-}CH_3\,(T_1) \rightarrow HC^{\bullet}O + HOOC^{\bullet}H\text{-}CH_3 \qquad (R.iv)$$

For the lowest-lying conformer of T_1, reaction (R.iii) faces a CCSD(T)-F12 computed potential energy barrier of 2.3 kcal mol^{-1} but involving a quite rigid transition state **TS2**, whereas reaction (R.iv) has to clear a barrier of 4.1 kcal mol^{-1} over a fairly loose transition state **TS3**, such that the calculated rate of reaction (R.iv) at 18 kcal mol^{-1} internal energy is 2.4 × 10^{12} s^{-1}, substantially higher than the rate of 3.0 × 10^{11} s^{-1} of reaction (R.iii). Interestingly, the barrier for the dissociation (R.iv) of 4.1 kcal mol^{-1} is much lower than the 12.6 kcal mol^{-1} derived from experiment[42] for the analogous dissociation of triplet acetaldehyde; this can be ascribed to the strong energy-stabilizing effects of primarily OOH and to a lesser extent also the CH_3 substituent on the resulting $HOOC^{\bullet}H\text{-}CH_3$ radical **5**. The more important reaction (R.iv) will be followed spontaneously by the barrierless decomposition of the unstable α-hydroperoxy alkyl radical[43] **5** into OH + CH_3CHO **6**, and as such should be a source of (recycled) hydroxyl radicals:

$$HOOC^{\bullet}H\text{-}CH_3 \rightarrow OH + CH_3CHO \qquad (R.v)$$

Given the very high rate of (R.iv), it is clear that the ISC $S_1 \rightarrow T_1$ should be the rate-limiting step of this mechanism as it is highly unlikely to be as fast as 2 × 10^{12} s^{-1}. Accurate

View Article Online
DOI: 10.1039/C7CP08421H
PCCP ARTICLE

ab initio calculation of the ISC rate for 2-HPP — as well as that of the internal conversion (IC), $S_1 \rightarrow S_0^\dagger$ — remains a challenging task, beyond the scope of this article. However, from available product data on the photolysis of propanal, it can be construed that in the range 290 - 320 nm intersystem crossing $S_1 \rightarrow T_1$ occurs for that aldehyde at a rate (somewhat) above 10^{10} s^{-1}, whereas IC is minor compared to ISC. The key experimental findings in this respect are that the HCO + C_2H_5 product quantum yield is close to 1.0 up to a pressure of 1 atm.[40] At that pressure collisional stabilization of $S_1^\dagger$, $T_1^\dagger$ or $S_0^\dagger$, each of which is potentially competitive with a route to the products, occurs at a rate of order 10^9 s^{-1}. The above then implies that the rate of the major photolysis pathway(s) must be $\geq 10^{10}$ s^{-1}. On the other hand, for internal energies around 95 kcal mol^{-1} of the $S_0^\dagger$ formed via IC and for a C_2H_5-CHO dissociation energy of ≈83 kcal mol^{-1}, the impulsive dissociation rate $S_0^\dagger \rightarrow$ HCO + C_2H_5 is well below 10^7 s^{-1}, meaning that any $S_0^\dagger$ would instead be collisionally stabilized at 1 atm and the quantum yield through IC should be zero. Given the experimental quantum yield of 1.0, IC is therefore minor and ISC should be the dominant photolysis route, with rate of order 10^{10} s^{-1}.

Thus, unless the rate of ISC for the $S_1^\dagger$ of 2-HPP is at least $\approx 5 \times 10^{10}$ s^{-1}, a lesser fraction of the initially formed $S_1^\dagger$ is expected to undergo the sequence (R.ii), (R.iv) and (R.v) and so (re)generate OH, whereas reaction (R.i) forming singlet O_2 and the enol HOCH=CH-CH_3 should be major.

In principle, another possible photolysis mechanism yielding OH is internal conversion of the excited singlet state S_1 to the ground state $S_0^\dagger$ that then arises with a high vibrational energy content of nearly 92 kcal mol^{-1}, sufficient for its impulsive dissociation into OH + OCH-CH($O^\bullet$)-CH_3. Rupturing the RO-OH bond in organic hydroperoxides requires about 43 kcal mol^{-1}.[44] It should be followed by fast decomposition of the oxy radical into $HC^\bullet O$ + acetaldehyde, over a barrier of only ≈7.5 kcal mol^{-1} according to a pertaining Structure Activity Relationship.[45] However, the major bottleneck for this process is expected to be the initial IC, which for the propanal analogue was estimated above to be minor compared to the ISC, and is therefore unlikely to be of importance compared to the fast 1,5 H-shift (R.i) of 2-HPP-S_1 and the ISC route through (R.iv).

Photolysis of Hydroperoxyacetone. The investigation of the photolysis of $CH_3C(O)CH_2OOH$ was limited to the 1,5 H-shift in the initially excited singlet S_1 state. The most stable, H-bonded conformer (analogous to 2-HPP(2a) S_1), was computed to lie 84.7 kcal mol^{-1} above the S_0 state at the TD-M06-2X-D3 level, while the barrier to the 1,5 H-shift was found to be 1.3 kcal mol^{-1}, which is close to the barrier in 2-HPP. For an average total initial energy of S_1 of 92 kcal mol^{-1}, the rate of the activated 1,5 H-shift was evaluated at 3.3×10^{11} s^{-1}. Since the methyl substituent is not directly involved in the subsequent O_2 elimination to form an enol, it can reasonably be assumed that this process occurs spontaneously as found for the smaller hydroperoxyacetaldehyde $OCHCH_2OOH$.

Therefore, unless the ISC to T_1 is as fast as $\geq 5 \times 10^{10}$ s^{-1}, the direct reaction of S_1 is expected to be the major photolysis channel similar to the α-hydroperoxyaldehydes.

Photolysis rates. The measured absorption cross sections of hexyl-ketohydroperoxides in acetonitrile[1] are displayed in Figure 4(a) (red and green diamonds). Their cross sections in the gas phase (red and green curves) were estimated from their values in solution by assuming that they are similarly enhanced and red-shifted as those of acetone, also measured by Jorand et al.[1] in acetonitrile; that is, the gas-phase cross sections are assumed equal to the cross sections in solution red-shifted by 10 nm and enhanced by a factor of 1.4. In the case of acetone, this procedure reproduces the gas-phase experimental cross sections[46] to within 8% between 300 and 330 nm (Figure S10). Note that the cross sections in acetonitrile of hydrogen peroxide below 290 nm[1] as well as of other carbonyls (such as MACR)[26] were also found to be lower, and blue-shifted compared to their gas-phase counterparts. Alternative extrapolation procedures (Figure S10) providing a better fit of the acetone cross section maximum below 300 nm (but underestimating the cross sections at higher wavelengths) were also tested and found to provide similar results (within 15%) for the ketohydroperoxides. Nevertheless, the uncertainty associated to the extrapolation is acknowledged to be large and difficult to assess; unfortunately, the cross sections of hydroperoxides in acetonitrile at the relevant wavelengths (>320 nm) are not known.

View Article Online
DOI: 10.1039/C7CP08421H

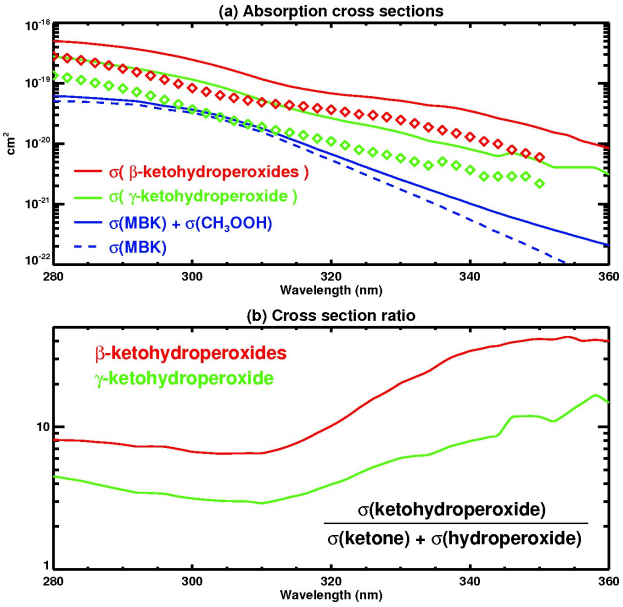

Figure 4. (a) Absorption cross sections of the mixture 2-4- and 3,5-hexylketohydroperoxide (red) and 2,5-hexylketohydroperoxide (green), both measured in acetonitrile by Jorand et al. (diamonds) and estimated in the gas phase (curves). Also shown are the measured gas-phase cross sections of methylbutylketone (MBK, dashed blue line) and the sum of the cross sections of MBK and CH_3OOH (solid blue line). (b) Ratio of the gas-phase cross sections of the ketohydroperoxides over the sum of the cross sections of MBK and CH_3OOH. β-ketohydroperoxides: 2-4- and 3,5-hexylketohydroperoxide; γ-ketohydroperoxide: 2,5-hexylketohydroperoxide.

As seen on Figure 4, the cross sections of the ketohydroperoxides are much higher than the sum of the cross sections of the most closely similar monofunctional compounds, methylbutylketone[47] and methylhydroperoxide.[48] Their enhancement ratio, defined by

$$r_{kh} = \frac{S_{kh}}{S_k + S_h}$$

where S_{kh}, S_k and S_h denote the cross sections of the ketohydroperoxide and of the monofunctional ketone and hydroperoxide, respectively, are largest at high wavelengths, up to a factor of 40 for β-ketohydroperoxides and a factor of ~10 for the γ-ketohydroperoxide (Figure 4(b)). This enhancement is due to the interaction between the two functional groups, and shows some similarities with enhancements observed for nitrooxycarbonyls.[25] For hydroperoxycarbonyls, the intrinsically "forbidden" character of the carbonyl (n,π*) transition might be relaxed by the neighbouring –OOH group. H-bonding likely plays a key role in enhancing the transition probability (through a larger overlap integral), as indicated by the much larger cross sections of β- compared to γ-ketohydroperoxides. Indeed, the 7-membered H-bonded rings formed from the H-bonding of the carbonyl-O and hydroperoxide-H in β-hydroperoxycarbonyls are significantly more stable than the 8-membered H-bonded rings in γ-hydroperoxycarbonyls as ring strain is expected to be larger for 8-rings compared to 6-and 7-rings.[49] The H-bonded fraction is therefore expected to be larger for β- compared to γ-hydroperoxycarbonyls. In the absence of additional experimental data, the cross section enhancements for α-hydroperoxycarbonyls is expected to be of the same order as for β-hydroperoxycarbonyls, because the marginally lower stability of H-bonded 6-rings compared to 7-rings (by 0 to 1 kcal mol^{-1}) should be roughly compensated by a higher (entropic) prefactor.

Following a similar methodology as for the cross sections of carbonyl nitrates,[25] we propose to calculate the absorption cross sections (S_{ch}) of a carbonyl hydroperoxide using

$$S_{ch} = (S_c + S_h) \cdot r_{kh}$$

where S_c denotes the measured cross sections of a monofunctional carbonyl structurally similar to the carbonyl hydroperoxide, S_h represents the cross sections of CH_3OOH (given the general absence of other cross section data for organic hydroperoxides), and r_{kh} is the cross section enhancement as defined above. All α- and β-hydroperoxycarbonyls are assumed to have the same enhancements as those derived for the β-ketohydroperoxides of Jorand et al. (Figure 4(b)).[1] This procedure is illustrated in Figure 5 for several important α-hydroperoxycarbonyls. Assuming wavelength-independent quantum yields, the photolysis rates calculated using the Tropospheric Ultraviolet and Visible (TUV) model[50] are increased by factors of 12-13 compared to calculations using the sum (S_c + S_h). Hydroperoxyaldehydes are estimated to photolyze about three times faster than the hydroperoxyketones, assuming identical quantum yields. The major uncertainties in these estimations arise from (1)

View Article Online
DOI: 10.1039/C7CP08421H
PCCP ARTICLE

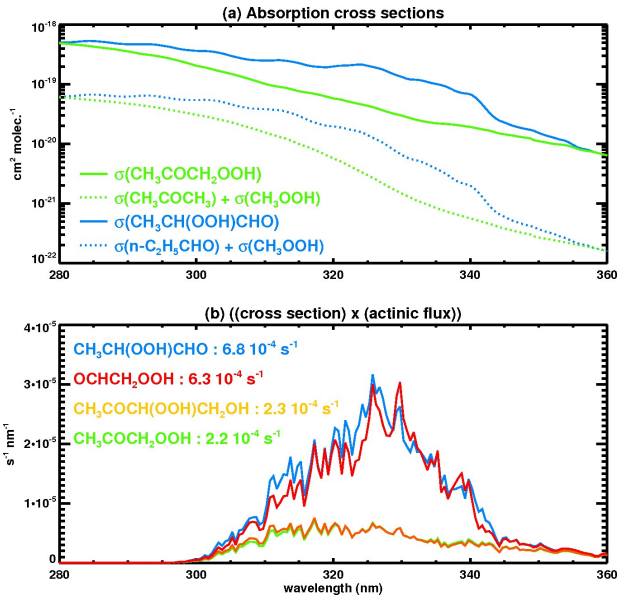

Figure 5. (a) Cross sections of hydroperoxyacetone and hydroperoxypropanal (solid lines) estimated as described in the text, and sum of the measured cross sections of related monofunctional compounds (dotted lines). (b) Product of the absorption cross section and the actinic flux (in s^{-1} nm^{-1}) for different α-hydroperoxycarbonyls, calculated at the Earth's surface for a 30° solar zenith angle with 300 DU ozone. The estimated photorates assuming unit quantum yield are also given.

the extrapolation from the solvent to the gas phase of the ketohydroperoxide cross sections, and (2) the assumption that the enhancement r_{kh} is valid for all α-hydroperoxycarbonyls.

This estimation method is evaluated against the measured photolysis rate of the hydroxy-ketohydroperoxide $CH_3C(=O)CH(OOH)CH_2OH$ in the 1 m^3 Caltech chamber.[14] The experiment used blacklights (8 Sylvania 350BL) irradiating above 300 nm, with a maximum at 354 nm.[51] Convolution of the actinic flux spectrum (Figure S11(a)) with the cross sections estimated as described above, based on the cross sections of methylethylketone[47,52] and CH_3OOH, leads to a chamber photolysis rate estimate of 5.3×10^{-5} s^{-1} when assuming a unit quantum yield (Figure S11(b,c)). Considering the large uncertainties in the cross sections, this estimate is broadly consistent with the measured rate (3.0×10^{-5} s^{-1}).[14] The latter can be reproduced by assuming a quantum yield close to 0.57 or, equally well, by a near-unit quantum yield in combination with lower cross sections. Note that without the cross-section enhancement, the photolysis rate estimate would be only 2.5×10^{-6} s^{-1}, more than an order of magnitude below the measured value even when assuming a unit quantum yield. The large cross-section enhancements revealed in acetonitrile[1] are clearly indispensable to explain the high measured α-hydroperoxyketone photolysis rate in the gas phase. Considering the limited data at our disposition, it appears reasonable to recommend to adopt a near-unit quantum yield (0.8) and cross sections estimated as above, but further multiplied by 0.7 in order to match the only experimental photolysis rate data.

Atmospheric implications. Adopting typical daytime atmospheric conditions, photolysis is calculated to be a major sink for all hydroperoxycarbonyls (Table 2). For all hydroperoxyaldehydes and for several key hydroperoxyketones, photolysis is even largely dominant, e.g. it represents ~78% of the total photochemical sink for hydroperoxyacetone and hydroperoxyacetaldehyde, both known to be formed in the oxidation of isoprene.[18] The formation of hydroperoxycarbonyls in the atmosphere leads thus probably to a lower consumption of OH radicals than currently implied by chemical mechanisms (such as the MCM[53]) for which the reaction with OH is largely dominant. The overall net impact on OH is difficult to assess, also since the atmospheric fate of enols remains unclear. A possible major sink of enols might be their tautomerization into their more stable carbonyl form, following uptake by aqueous aerosols or cloud droplets.[54] In the case of vinyl alcohol HO-CH=CH_2, which we predict to be the likely major product of hydroperoxyacetaldehyde (HPAC) photolysis, tautomerization to acetaldehyde was estimated to be a sink about equally important as reaction with OH.[54] The latter was previously proposed[55-56] to lead to formic acid and glyoxal formation. Another suggested sink of enols is their reaction with the Criegee Intermediate $^{\bullet}CH2OO^{\bullet}$, which for vinyl alcohol was predicted to yield mainly formic acid and acetaldehyde.[57] Based on our current knowledge of HPAC formation in the oxidation of isoprene and acetaldehyde,[15,17-19,53] the HPAC global production is estimated to be of the order of 20 Tg/year (for global sources of 567 Tg/yr isoprene and 213 Tg/yr acetaldehyde). Considering only the reaction of vinyl alcohol with OH and its tautomerization and assuming them equally important,

View Article Online
DOI: 10.1039/C7CP08421H

Table 2. Sink rates of hydroperoxycarbonyls due to photolysis (J) and reaction with OH (k_{OH} × [OH])

compound	notation	J (s^{-1})	k_{OH} × [OH] (s^{-1})
$CH_3C(=O)CH(OOH)CH_2OH$	HMVKBOOH	1.3×10^{-4}	1.2×10^{-4}
$CH_3C(=O)CH_2OOH$	HYPERACET	1.27×10^{-4}	3.6×10^{-5}
$O=CHCH_2OOH$	HCOCH2OOH	3.6×10^{-4}	1.0×10^{-4}
$O=CHC(CH_3)(OOH)CH(OOH)CH_2OOH$	C536OOH	5.2×10^{-4}	2.0×10^{-4}
$CH_3C(=O)CH(OOH)CH_2OOH$	DIHPMEK	1.3×10^{-4}	8.8×10^{-5}
$O=CHC(CH_3)(OOH)CH_2OOH$	DIHPMPAL	5.2×10^{-4}	1.1×10^{-4}
$CH_3C(=O)CH(OOH)CH(=O)$	C4CO2OOH	2.6×10^{-4}	2.3×10^{-4}
$CH_3CH(OOH)CH(=O)$	PROPALOOH	3.9×10^{-4}	1.3×10^{-4}
$CH_3C(=O)CH_2CH_2OOH$	MEKAOOH	1.3×10^{-4}	1.5×10^{-4}
$CH_3C(=O)CH(OOH)CH_3$	MEKBOOH	1.3×10^{-4}	5.6×10^{-5}

Photolysis rates calculated with TUV for 30° solar zenith angle and 300 DU ozone. [OH] taken equal to 3×10^6 molec. cm^{-3}. Species notation and OH-rate constants from the MCMv3.3.1 (mcm.leeds.ac.uk/MCM).[53]

HPAC photolysis is estimated to form up to 4 Tg/yr acetaldehyde and 2.7 Tg/yr HCOOH globally.

Conclusions

In this theoretical investigation of the photolysis of α-hydroperoxycarbonyls:

1. We newly identified a fast 1,5 H-shift of the hydroperoxide-H to the carbonyl-O in the initially excited S_1 state of α-hydroperoxycarbonyls. At a computed overall rate of ≈5×10^{10} s^{-1} in atmospheric conditions, this reaction is most likely faster than intersystem crossing to the T_1 state and should be the major atmospheric photolysis route of the title compounds. Because of the high rate of the S_1 reaction, we expect the quantum yield in atmospheric conditions to approach unity.

2. We found that the H-shift is followed by spontaneous elimination of singlet O_2 to yield an enol, such that the overall process can be written as a type II Norrish mechanism:

$$OCR_1\text{-}C(OOH)R_2R_3 + h\nu \rightarrow {}^1O_2 + HO\text{-}CR_1{=}CR_2R_3$$

In the atmosphere, the enols should either react with OH or tautomerize into the more stable carbonyl compounds $O{=}CR_1\text{-}CHR_2R_3$ following uptake by aqueous aerosols,[54] or react with Criegee Intermediates.[57]

3. As a second photolysis route of α-hydroperoxycarbonyls, we identified and quantified the very fast two-step decomposition of the T_1 state following $S_1 \rightarrow T_1$ intersystem crossing:

$$OCR_1\text{-}C(OOH)R_2R_3 + h\nu \rightarrow R_1CO + OH + R_2C(O)R_3$$

4. Supported by evidence from the literature, we argue that the important enhancement of the absorption cross sections over those of the constituent monofunctional compounds as observed for the analogous β-ketohydroperoxides,[1] should also apply to α-hydroperoxycarbonyls. On this basis, and adopting the near-unity photolysis quantum yield found in this work, we predict atmospheric photolysis rates of α-hydroperoxycarbonyls of the order of (1 to 5) × 10^{-4} s^{-1}, in most cases outrunning their reactions with OH.

Acknowledgements

This work was sponsored in part by Belspo under contract SD/CS/05A (project BIOSOA) in the frame of the Science for Sustainable Development program. It also received support from grant #C14/15/052 by the KU Leuven, and the Office of China Postdoctoral Council (No. 20140061) through the International Postdoctoral Exchange Fellowship Program. We acknowledge the Flemish Supercomputer Centre (VSC) and the supercomputer at ECUST Shanghai for generous computing resources.

View Article Online
DOI: 10.1039/C7CP08421H

References

1 F. Jorand, L. Kerhoas, A. Heiss, J. Einhorn and K. Sahetchian, *J. Photochem. Photobiol. A: Chem.*, 2000, **134**, 119-125.

2 J. Seinfeld, and S. N. Pandis, Atmos. Chem. Phys.: From Air Pollution to Climate Change, 3d edition, 2016, John Wiley and sons, New York, 1152 pp.

3 B. Aumont, S. Madronich, I. Bey and G. S. Tyndall, *J. Atmos. Chem.*, 2000, **35**, 59-75.

4 M. E. Jenkin, *Atmos. Chem. Phys.*, 2004, **4**, 1741-1757.

5 B. Bonn, R. von Kuhlmann and M. G. Lawrence, *Geophys. Res. Lett.*, 2004, **31,** L10108, doi:10.1029/2003GL019172.

6 M. Capouet, J. F. Müller, K. Ceulemans, S. *Compernolle*, L. Vereecken and J. Peeters, *J. Geophys. Res.*, 2008, **113**: D02308, doi:10.1029/2007JD008995.

7 M. Capouet and J. F. Müller, *Atmos. Chem. Phys.*, 2006, **6**, 1455-1467.

8 T. Raventos-Duran, M. Camredon, R. Valorso, C. Mouchel-Vallon and B. Aumont, *Atmos. Chem. Phys.*, 2010, **10**, 7643-7654.

9 J. Peeters, T. L. Nguyen and L. Vereecken, *Phys. Chem. Chem. Phys.*, 2009, **11**, 5935-5939.

10 J. D. Crounse, F. Paulot, H. G. Kjaergaard and P. O. Wennberg, *Phys. Chem. Chem. Phys.*, 2011, **13**, 13607-13613.

11 J. D. Crounse, L. B. Nielsen, S. Jørgensen, H. G. Kjaergaard *and* P. O. Wennberg, *J. Phys. Chem. Lett.*, 2013, **4**, 3513-3520.

12 M. Ehn, J. A. Thornton, E. Kleist, M. Sipila, H. Junninen, I. Pullinen, M. Springer, F. Rubach, R. Tillmann, B. Lee, F. Lopez-Hilfiker, S. Andres, I. H. Acir, M. Rissanen, T. Jokinen, S. Schobesberger, J. Kangasluoma, J. Kontkanen, T. Nieminen, T. Kurten, L. B. Nielsen, S. Jorgensen, H. G. Kjaergaard, M. Canagaratna, M. D. Maso, T. Berndt, T. Petaja, A. Wahner, V. M. Kerminen, M. Kulmala, D. R. Worsnop, J. Wildt and T. F. Mentel, *Nature*, 2014, **506**, 476-479.

13 T. Jokinen, T. Berndt, R. Makkonen, V. M. Kerminen, H. Junninen, P. Paasonen, F. Stratmann, H. Herrmann, A. B. Guenther, D. R. Worsnop, M. Kulmala, M. Ehn and M. Sipila, *Proc. Natl. Acad. Sci. U.S.A*, 2015, **112**, 7123-7128.

14 E. Praske, J. D. Crounse, K. H. Bates, T. Kurten, H. G. Kjaergaard and P. O. Wennberg, *J. Phys. Chem. A*, 2015, **119**, 4562-4572.

15 J. M. St Clair, J. C. Rivera-Rios, J. D. Crounse, H. C. Knap, K. H. Bates, A. P. Teng, S. Jorgensen, H. G. Kjaergaard, F. N. Keutsch and P. O. Wennberg, *J. Phys. Chem. A*, 2016, **120**, 1441-1451.

16 T. Berndt, H. Herrmann, M. Sipila and M. Kulmala, *J. Phys. Chem. A*, 2016, **120**, 10150-10159.

17 R. H. Schwantes, A. P. Teng, T. B. Nguyen, M. M. Coggon, J. D. Crounse, J. M. St Clair, X. Zhang, K. A. Schilling, J. H. Seinfeld and P. O. Wennberg, *J. Phys. Chem. A*, 2015, **119**, 10158-10171.

18 A. P. Teng, J. D. Crounse and P. O. Wennberg, *J. Am. Chem. Soc.*, 2017, **139**, 5367-5377.

19 J. Peeters, J. F. Muller, T. Stavrakou and V. S. Nguyen, *J. Phys. Chem. A*, 2014, **118**, 8625-8643.

20 S. M. Saunders, M. E. Jenkin, R. G. Derwent and M. J. Pilling, *Atmos. Chem. Phys.*, 2003, **3**, 161-180.

21 A. Hodzic, S. Madronich, P. S. Kasibhatla, G. Tyndall, B. Aumont, J. L. Jimenez, J. Lee-Taylor and J. Orlando, *Atmos. Chem. Phys.*, 2015, **15**, 9253-9269.

22 J. Peeters and J. F. Muller, *Phys. Chem. Chem. Phys.*, 2010, **12**, 14227-14235.

23 G. M. Wolfe, J. D. Crounse, J. D. Parrish, J. M. St Clair, M. R. Beaver, F. Paulot, T. P. Yoon, P. O. Wennberg and F. N. Keutsch, *Phys. Chem. Chem. Phys.*, 2012, **14**, 7276-7286.

24 R. Suarez-Bertoa, B. Picquet-Varrault, W. Tamas, E. Pangui and J. F. Doussin, *Environ. Sci. Technol.*, 2012, **46**, 12502-12509.

25 J. F. Müller, J. Peeters and T. Stavrakou, *Atmos. Chem. Phys.*, 2014, **14**, 2497-2508.

26 F. Xiong, C. H. Borca, L. V. Slipchenko and P. B. Shepson, *Atmos. Chem. Phys.*, 2016, **16**, 5595-5610.

27 J. W. Ponder, and F. M. Richards, *J. Comput. Chem.*, 1987, **8**, 1016-1024.

28 Gaussian 09, Revision E.01, M. J. Frisch, G. W. Trucks, H. B. Schlegel, G. E. Scuseria, M. A. Robb, J. R. Cheeseman, G. Scalmani, V. Barone, B. Mennucci, G. A. Petersson, H. Nakatsuji, M. Caricato, X. Li, H. P. Hratchian, A. F. Izmaylov, J. Bloino, G. Zheng, J. L. Sonnenberg, M. Hada, M. Ehara, K. Toyota, R. Fukuda, J. Hasegawa, M. Ishida, T. Nakajima, Y. Honda, O. Kitao, H. Nakai, T. Vreven, J. A. Montgomery, Jr., J. E. Peralta, F. Ogliaro, M. Bearpark, J. J. Heyd, E. Brothers, K. N. Kudin, V. N. Staroverov, R. Kobayashi, J. Normand, K. Raghavachari, A. Rendell, J. C. Burant, S. S. Iyengar, J. Tomasi, M. Cossi, N. Rega, J. M. Millam, M. Klene, J. E. Knox, J. B. Cross, V. Bakken, C. Adamo, J. Jaramillo, R. Gomperts, R. E. Stratmann, O. Yazyev, A. J. Austin, R. Cammi, C. Pomelli, J. W. Ochterski, R. L. Martin, K. Morokuma, V. G. Zakrzewski, G. A. Voth, P. Salvador, J. J. Dannenberg, S. Dapprich, A. D. Daniels, Ö. Farkas, J. B. Foresman, J. V. Ortiz, J. Cioslowski, and D. J. Fox, Gaussian, Inc., Wallingford CT, 2009.

29 F. *Neese*, *WIREs Comput. Mol. Sci.*, 2012, **2**, 73-78.

View Article Online
DOI: 10.1039/C7CP08421H

30 H. J. Werner, P. J. Knowles, G. Knizia, F. R. Manby, and M. Schütz, *WIREs Comput. Mol. Sci.*, 2012, **2**, 242-253.

31 W. *Forst*, Theory of Unimolecular Reactions, Academic Press, New York, 1973.

32 K. A. Holbrook, M.J. Pilling, and S.H. Robertson, *Unimolecular* Reactions (2nd ed.), John Wiley & Sons, New York, 1996.

33 H. Liu, E. C. Lim, R. H. Judge and D. C. Moule, *J. Chem. Phys.*, 1995, **102**, 4315-4320.

34 H. Liu, E. C. Lim, C. Muñoz‐Caro, A. Niño, R. H. Judge and D. C. Moule, *J. Chem. Phys.*, 1996, **105**, 2547-2552.

35 T. Gejo, H. Bitto and J. R. Huber, *Chem. Phys. Lett.*, 1996, **261**, 443-449.

36 S.-H. *Lee* and I. C. Chen, *Chem. Phys.*, 1997, **220**, 175-189.

37 A. *Horowitz*, C. J. Kershner and J. G. Calvert, *J. Phys. Chem.,* 1982, **86**, 3094-3105.

38 T. Kono, M. Takayanagi, T. Nishiya and I. Hanazaki, *Chem. Phys. Lett.*, 1993, **201**, 166-170.

39 S. H. Lee and I. C. Chen, *J. Chem. Phys.*, 1996, **105**, 4597-4604.

40 Y. Chen and L. Zhu, *J. Phys. Chem. A*, 2001, **105**, 9689-9696.

41 Y. Chen, L. Zhu and J. S. Francisco, *J. Phys. Chem. A*, 2002, **106**, 7755-7763.

42 G.-H. Leu, C.-L. Huang, S.-H. Lee, Y.-C. Lee and I. C. Chen, *J. Chem. Phys.*, 1998, **109**, 9340-9350.

43 L. Vereecken, T. L. Nguyen, I. Hermans and J. Peeters, *Chem. Phys. Lett.*, 2004, **393**, 432-436.

44 J. Matthews, A. Sinha and J. S. Francisco, *J. Chem. Phys.*, 2005, **122**, 221101.

45 L. Vereecken and J. Peeters, *Phys. Chem. Chem. Phys.*, 2009, **11**, 9062-9074.

46 T. Gierczak, J. B. Burkholder, S. Bauerle and A. R. Ravishankara, *Chem. Phys.*, 1998, **231**, 229-244.

47 R. D. Martinez, A. A. Buitrago, N. W. Howell, C. H. Hearn and J. A. Joens, *Atmos. Environ. Part A*, 1992, **26**, 785-792.

48 G. L. *Vaghjiani* and A. R. Ravishankara, *J. Geophys. Res.*, 1989, **94**, 3487-3492.

49 J. B. Pedley, Thermochemical Data and Structures of Organic Compounds, Volume I, Thermodynamics *Research* Center, College Station, Texas, 1994.

50 S. Madronich, and S. Flocke, in Handbook of *Environmental* Chemistry, 1998, P. Boule, ed., Springer-Verlag, Heidelberg, 1-26.

51 W. *Carter*, D. Cockeriii, D. Fitz, I. Malkina, K. Bumiller, C. Sauer, J. Pisano, C. Bufalino and C. Song, *Atmos. Environ.*, 2005, **39**, 7768-7788.

52 J. *Chen* and D. S. Venables, *Atmos. Meas. Tech.*, 2011, **4**, 425-436.

53 M. E. Jenkin, J. C. Young and A. R. Rickard, *Atmos. Chem. Phys.*, 2015, **15**, 11433-11459.

54 J. *Peeters*, V. S. Nguyen and J. F. Muller, *J. Phys. Chem. Lett.*, 2015, **6**, 4005-4011.

55 A. T. Archibald, M. R. McGillen, C. A. Taatjes, C. J. Percival and D. E. Shallcross, *Geophys. Res. Lett.*, 2007, **34:** L21801, doi:10.1029/2007GL031032.

56 S. So, U. Wille and G. da Silva, *Environ. Sci. Technol.*, 2014, **48**, 6694-6701.

57 A. Jalan, I. M. Alecu, R. Meana-Pañeda, J. Aguilera-Iparraguirre, K. R. Yang, S. S. Merchant, D. G. Truhlar and W. H. Green, *J. Am. Chem. Soc.*, 2013, **135**, 11100−11114.

